Quantum Electronics **40** (5) 411 – 417 (2010)

LIGHT SCATTERING AND RADIATION TRANSMISSION THROUGH ATMOSPHERE

PACS numbers: 42.25.Fx; 33.50.–j; 07.05.Pj
DOI: 10.1070/QE2010v040n05ABEH014319

Scattering effect on the imaging depth limit in two-photon fluorescence microscopy

E.A. Sergeeva

***Abstract*. A model for the propagation of a focused light beam in a strongly scattering medium is used to analyse various factors that limit the capability of two-photon fluorescence microscopy (TPFM) to image deep sections of optically thick biological specimens. The TPFM imaging depth is shown to be limited by three main factors: (1) beam broadening as a result of multiple small-angle scattering, leading to a loss of submicron lateral resolution; (2) strong near-surface fluorescence at large imaging depths as a result of the increase in average source power in order to compensate for scattering losses; (3) reduction in useful two-photon fluorescence signal level because of the exponential attenuation of the excitation power. The influence of these factors is examined in a small-angle diffusion approximation of radiative transfer theory. The first two of them are shown to set a fundamental TPFM limit, whereas the last is an instrumental limitation and appears to be the most critical to state-of-the-art commercial two-photon laser scanning microscopy systems for the vast majority of fluorophores in current use.**

Keywords: *two-photon fluorescence microscopy, multiple scattering, radiative transfer theory, small-angle diffusion approximation.*

1. Introduction

Two-photon fluorescence microscopy (TPFM), first proposed and implemented in 1990 as a modernisation of laser scanning microscopy [1], is among the most promising techniques for submicron-resolution three-dimensional (3D) imaging of the structure of strongly scattering objects (predominantly of biological tissues) [1 – 4]. In this method, a fluorophore in the specimen to be studied is nonlinearly excited through absorption of two photons in the range 700 – 1000 nm, followed by emission of a photon in the visible range. Compared to confocal laser microscopy, TPFM offers a greater imaging depth in biological tissues [3 – 6], with spatial resolution at the level of a fraction of a micron and high image contrast even without pinhole detection. These advantages are ensured by excitation with near-IR radiation, which is more weakly scattered in biological tissues than is visible light, and by the localisation of the two-photon fluorescence excitation within the focal volume of a highly focused excitation beam, i.e., in the peak intensity region. The two-photon excitation of fluorophores in biological specimens is usually provided by femtosecond pulses of Ti : sapphire laser sources tunable in the wavelength range 700 – 1000 nm, with a pulse duration of about 100 fs and a repetition rate of about 100 MHz. At an average power in the focal volume below 10 mW, the pulse peak power reaches kilowatts, which enables effective excitation of both highly fluorescent chemical markers and weakly fluorescent endogenous fluorophores [3, 7].

At the same time, the imaging depth limit in TPFM is substantially smaller than that in optical coherence tomography (OCT), another method widely used for micron-resolution imaging of the structure of biological tissues. The OCT imaging depth is known to be limited by multiple small-angle scattering effects and the increased contribution of large-angle scattering. These effects are important at depths exceeding 10 – 15 photon mean free paths between individual scattering events, i.e. exceeding the transport length [8, 9]. In the transmission window 600 – 1200 nm, this quantity ranges from several hundred microns in dense biological tissues and skin to millimetres in mucous tissue [10]. At the same time, when conventionally stained specimens are examined using a typical commercial laser scanning microscopy system, the maximum TPFM imaging depth does not exceed 600 μm [4, 5]. This implies that the broadening of the focused beam is not the main factor limiting the TPFM imaging depth.

The TPFM imaging depth may also be limited by strong near-surface fluorescence. The unscattered light power at the excitation beam focus in a turbid medium drops exponentially, following the Lambert – Beer law [11]. To compensate for these losses, the excitation power in the focal volume should be raised at least to the milliwatt level. The local excitation intensity far away from the focal point but near the specimen surface may then approach the focal intensity, which may cause images corresponding to different depths to superimpose on one another. Theer and Denk [12] suppose that the TPFM imaging depth is ultimately limited by near-surface fluorescence. The attenuation of the useful signal because of the exponential drop in its power may however be a more stringent limitation.

This paper analyses all the above factors limiting the TPFM imaging depth in scattering media. The main factor limiting the imaging depth is identified for various types of

E.A. Sergeeva Institute of Applied Physics, Russian Academy of Sciences, ul. Ul'yanova 46, 603950 Nizhnii Novgorod, Russia; e-mail: sea@ufp.appl.sci-nnov.ru

Received 26 February 2010; revision received 8 April 2010
Kvantovaya Elektronika **40** (5) 411 – 417 (2010)
Translated by O.M. Tsarev

fluorophores, and the imaging depth is estimated. The effect of multiple small-angle scattering on the shape of a focused beam is examined within a small-angle diffusion approximation, which is applicable when the beam divergence exceeds the width of the small-angle part of the scattering phase function. The numerical characteristics used in the present calculations correspond to state-of-the-art commercial two-photon laser scanning microscopy systems.

2. Materials and characterisation techniques

2.1 Calculation of the two-photon fluorescence signal

The feasibility of nonlinear excitation of a fluorophore at wavelength λ_{ex} can be quantified using the two-photon absorption cross section, $\Sigma_2(\lambda_{ex})$, measured in cm^4 s $photon^{-1}$ [13]. Two-photon fluorescence calculations more often use the two-photon action cross section, Σ_2^*, equal to the product of Σ_2 and the two-photon fluorescence quantum yield. Near-IR Σ_2^* spectra have been measured for a wide range of organic fluorophores that are used in TPFM. The two-photon absorption cross section ranges from 10^{-3} GM (1GM = 10^{-50} cm^4 s $photon^{-1}$) in endogenous biological fluorophores (riboflavin, NADH) to 10^4 GM in colloidal quantum dots [2, 14, 15]. As shown by Xu and Webb [13], the number of fluorescence photons emitted per unit time from the focal volume of a focused femtosecond laser beam can be found as

$$u = \frac{\alpha \Sigma_2^* P_{ex}^2}{2\tau F} C_0 \int_V I_{ex}^2(\boldsymbol{r}) \mathrm{d}\boldsymbol{r}, \tag{1}$$

where P_{ex} is the average excitation power (measured in photons s^{-1}, like u); τ is the excitation pulse duration; α is the pulse shape factor ($\alpha = 1$ for a rectangular pulse and $\alpha = 0.4$ for a Gaussian pulse); F is the pulse repetition rate; C_0 is the fluorophore concentration averaged over the focal volume; and I_{ex} is the focal intensity profile of an excitation beam of unit power, which meets the normalisation condition $\int I_{ex}(\boldsymbol{r}_\perp, z)\mathrm{d}^2\boldsymbol{r}_\perp = 1$ (Fig. 1). Relation (1) is valid for nonscattering media and does not take into account two-photon absorption saturation effects. If a beam focused to depth z_f has the Gaussian intensity profile

$$I_{ex}(\boldsymbol{r}) = \exp\left(-\frac{\boldsymbol{r}_\perp^2}{S_0(z)}\right)[\pi S_0(z)]^{-1}, \tag{2}$$

where

$$S_0(z) = \left(0.61\frac{\lambda_{ex}}{\mathrm{NA}}\right)^2 + \frac{(z - z_f)^2 \mathrm{NA}^2}{(1.22\pi n)^2}$$

is the square of the 1/e diameter of the Gaussian beam at different z levels; n is the refractive index of the medium and NA is the numerical aperture of the focusing objective, relation (1) takes the form

$$u = \frac{\alpha \Sigma_2^* P_{ex}^2}{2\tau F} C_0 \frac{\pi n}{\lambda_{ex}}. \tag{3}$$

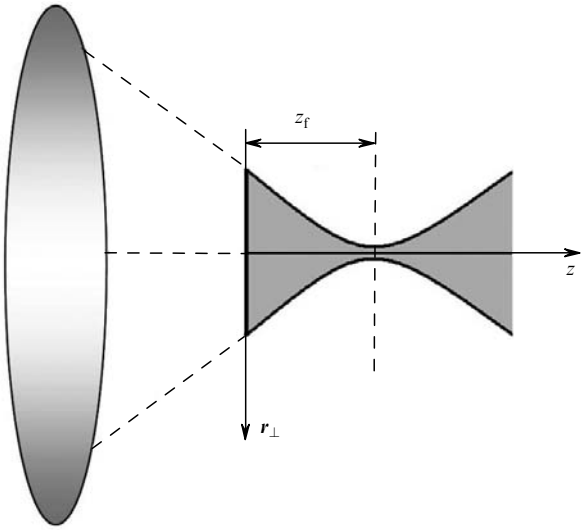

Figure 1. Geometry of the focused excitation beam.

The two-photon fluorescence signal measured by a photodetector is proportional to the product of the number of photons, u, and the collection efficiency of the detector system, which depends on the numerical aperture of the objective, the transmittance of the optical components and the size of the confocal pinhole at the detector [16, 17]. To describe the two-photon fluorescence signal from a scattering medium at the maximum size of the confocal pinhole, it is sufficient to examine the scattering effect on the fluorescence excitation efficiency. To this end, (2) and (3) should be corrected to include the excitation intensity attenuation by single scattering events and the effect of multiply scattered photons.

2.2 Imaging depth limit set by excitation beam broadening

Scattering causes photons to deviate from their original trajectories, leading to beam broadening at large depths. The propagation of a focused beam in a strongly scattering medium can be described analytically in terms of the radiative transfer theory [11]. The scattered beam intensity in soft biological tissues, where small-angle scattering of near-IR radiation prevails, can be determined in the small-angle diffusion approximation of the radiative transfer theory [18, 19]. The variance of the small-angle part of the scattering phase function, $\langle\theta^2\rangle$, for biological tissues is typically within 0.2 [10], and linear absorption effects can be neglected at lengths of up to several millimetres. When the numerical aperture of the objective lens is above 0.5, the width of the angular photon distribution exceeds that of the forward-scattering lobe of the scattering phase function for biological tissues, and the small-angle diffusion approximation can be used even at small scattering depths. We will take advantage of a refined small-angle diffusion approximation, in which the total beam intensity at depth z in a scattering medium with a scattering coefficient μ_s is the sum of the attenuated unscattered light intensity (ballistic component) and the scattered component [20]:

$$I = \mathrm{e}^{-\mu_s z} \exp\left(-\frac{\boldsymbol{r}_\perp^2}{S_0(z)}\right)[\pi S_0(z)]^{-1} +$$

$$+(1-\mathrm{e}^{-\mu_s z})\exp\left(-\frac{\boldsymbol{r}_\perp^2}{S_s(z)}\right)[\pi S_s(z)]^{-1}. \quad (4)$$

Here, S_s is the variance of the scattered light distribution, which depends on parameters of the beam and medium:

$$S_s(z) = S_0(z) + \frac{1}{3}\frac{\mu_s\langle\theta^2\rangle z^3}{1-\mathrm{e}^{-\mu_s z}}. \quad (5)$$

Figure 2 illustrates the effect of focusing depth, z_f, on the net focal intensity and its two components, and Fig. 3 shows the transverse profiles of the intensity components around the focal point. At small focusing depths, the ballistic component prevails, but with increasing depth an increasingly larger fraction of the beam energy is converted to the scattered component. For $\mu_s z_f > 10$, the focal intensity is dominated by scattered photons. The spatial resolution of TPFM is determined by the beam waist width. In the region where the ballistic component prevails, the lateral resolution is determined by the diffraction limit, $0.61\lambda_{ex}/\mathrm{NA}$. At the depths where the scattered component prevails, the beam waist size is determined mainly by the transverse distribution of multiply scattered photons and considerably exceeds the diffraction limit (Fig. 3). The imaging depth where TPFM loses submicron resolution, z_1, can be estimated as the depth where the intensities of the ballistic and scattered components near the focal point are comparable. Then, we have

$$1+\frac{\mathrm{NA}^2}{1.1\lambda_{ex}^2}\mu_s\langle\theta^2\rangle z_1^3 \simeq \mathrm{e}^{\mu_s z_1}. \quad (6)$$

The value of z_1 depends on parameters of both the scattering medium and excitation beam, but these dependences cannot be obtained in analytical form because Eqn (6) is transcendental. The effect of scattering parameters on z_1 is analysed graphically in Section 3.

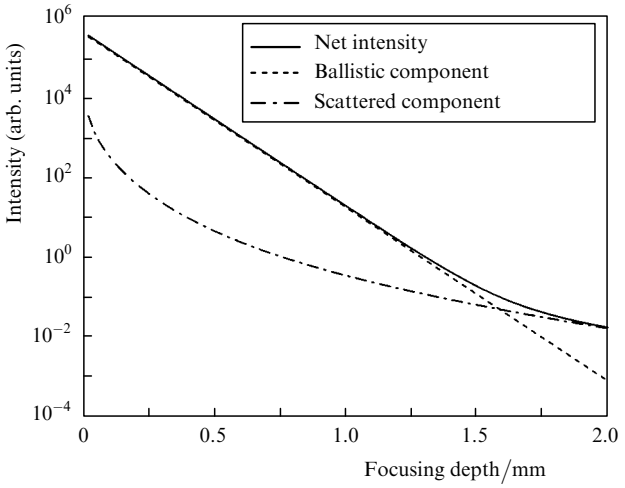

Figure 2. Intensity components at the waist of a highly focused excitation beam vs. focusing depth in a scattering medium. Excitation wavelength $\lambda_{ex} = 800$ nm; average refractive index of the medium $n = 1.33$; numerical aperture of the focusing objective NA = 0.8; scattering coefficient of the medium $\mu_s = 10\ \mathrm{mm}^{-1}$; scattering anisotropy factor $g = 0.95$.

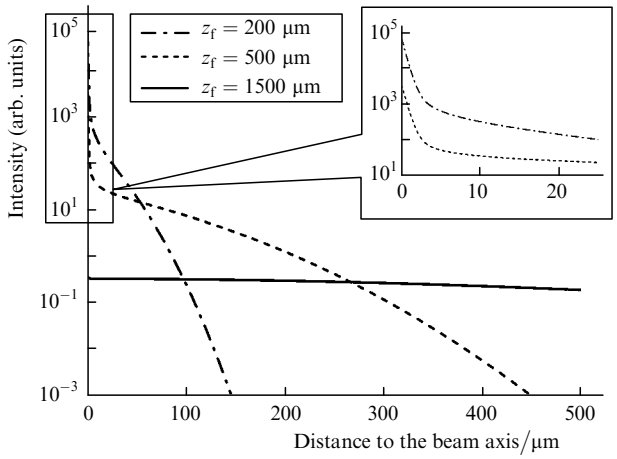

Figure 3. Transverse intensity profiles at the waist of a highly focused excitation beam at different focusing depths in a scattering medium; the same parameters of the beam and medium as in Fig. 2.

2.3 Imaging depth limit set by near-surface fluorescence

One of the key advantages of TPFM over confocal microscopy is that there is no background signal even without pinhole detection. In a transparent medium, only near the focal point is the local intensity high enough for effective nonlinear excitation of the fluorophore. In the case of larger imaging depths and strongly scattering media, it is necessary to compensate for the energy loss in the ballistic component and raise the incident beam power. This increases the near-surface intensity to an extent that the two-photon fluorescence excitation efficiency in the near-surface region approaches that around the focal point (Fig. 4), producing an additional image, which hinders the imaging of deeper layers [12, 21]. The focusing depth at which this effect becomes significant, z_2, can be determined from (4) by a numerical analysis of the net intensity profile along the beam axis. The plot of z_2 against the scattering coefficient of the medium is presented in Section 3.

2.4 Imaging depth limit set by the useful signal level

The above imaging depth limits are inherent to TPFM. These limits cannot be overcome by raising the excitation

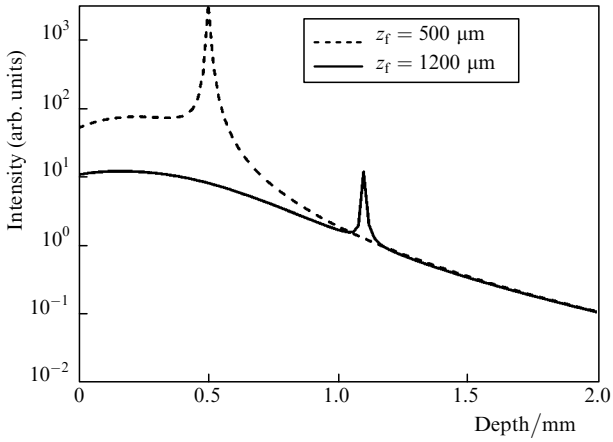

Figure 4. Intensity profiles along the axis of the excitation beam focused to different depths in a scattering medium; the same parameters of the beam and medium as in Fig. 2. At a focusing depth of 1200 μm, the focal intensity is comparable to the intensity at 300 μm depth.

power or enhancing the collecting power of the imaging system. They, however, may turn out to be secondary when the useful fluorescence signal is weak, approaching the detector noise level. In laser scanning microscopy, the contrast of an individual pixel is determined by the number of fluorescence photons detected during the signal acquisition from one point of the medium relative to the photodetector noise. The photodetector noise is mainly due to the shot effect, and its amplitude is proportional to the square root of the signal [22, 23]. To reach the minimum acceptable signal-to-noise ratio, the number of useful fluorescence photons per pixel, $N_{\min}$, must be at least ten [23]. The number of detected photons can be determined as the product of the number of fluorescence photons (3), the signal acquisition time per pixel (Δt) and the collecting power of the detector system (η). The last parameter depends on the numerical aperture of the objective lens, the transmission of the optical components in the fluorescence imaging system (dichroic mirrors and filters) and the size of the confocal pinhole at the detector. If a laser scanning microscopy system is equipped with a nondescanned detector* [21], the collecting power is determined mainly by the objective aperture and can be estimated as the fraction of fluorescence photons (with an isotropic angular distribution over the full solid angle 4π) in a cone with an opening angle $\alpha = \arcsin(\mathrm{NA})$:

$$\eta = \frac{2\pi(1-\cos\alpha)}{4\pi} = \frac{1-\sqrt{1-\mathrm{NA}^2}}{2}. \tag{7}$$

The number of useful photons that form an individual pixel can be found as

$$N = \frac{\alpha\Sigma_2^* C_0}{2\tau F}\frac{\pi n}{\lambda_{\mathrm{ex}}}P_{\mathrm{ex}}^2\frac{1-\sqrt{1-\mathrm{NA}^2}}{2}\Delta t. \tag{8}$$

Therefore, at particular parameters of the instrument (α, τ, F, λ_{ex}, NA, Δt) and fluorophore (C_0, Σ_2^*), the focal excitation power needed to produce the minimum necessary number of fluorescence photons is given by

$$P_{\mathrm{f}} = \left[\frac{\Delta t}{N_{\min}}\frac{\alpha\Sigma_2^* C_0}{2\tau F}\frac{\pi n}{\lambda_{\mathrm{ex}}}\frac{1-\sqrt{1-\mathrm{NA}^2}}{2}\right]^{-1/2}. \tag{9}$$

At the same time, the excitation power is limited by noninvasivity requirements. Laser safety standards [10] set the maximum energy density of short-time irradiation and the average laser radiation power for a given exposure time. The fluence 1 J cm^{-2} is considered a threshold above which various types of damage to biological tissues are possible, from thermal degradation to nonlinear optical breakdown, depending on the exposure time [6]. The energetic characteristics of a pulsed laser beam highly focused deep into a medium should meet two conditions: one must avoid optical breakdown by a single 100-fs pulse around the focal point, where the beam intensity is high, whereas on the specimen surface, where the intensity is low, one should prevent excessive overheating of the biological tissue by prolonged beam scanning over the same region. At a maximum permissible laser fluence of 0.1 J cm^{-2}, the average power in the waist should not exceed 10 mW, and that on the specimen surface at an exposure time of a fraction of a second should be no higher than several hundred milliwatts. This limit to the average power at the focal point correlates with experimental data [24, 25]: in TPFM examination of cell culture, beam powers above 10 mW lead to irreversible cell damage and mass death. In view of this, we will take $P_{\mathrm{f}}^* = 10$ mW as the maximum power at the focal point and $P_0^* = 100$ mW as the maximum permissible power on the specimen surface.

The focal power (at depth $z = z_{\mathrm{f}}$) in a scattering specimen and the power on its surface are related by the Lambert–Beer law [11]:

$$P_{\mathrm{f}} = P_0\exp(-\mu_{\mathrm{s}} z_{\mathrm{f}}). \tag{10}$$

As a result, the imaging depth limit set by the low useful signal level, z_3, can be evaluated from (9), (10) and the maximum power at the boundary:

$$z_3 = \frac{1}{\mu_{\mathrm{s}}}\ln\left[\frac{P_0^*}{P_{\mathrm{f}}}\right] = \frac{1}{\mu_{\mathrm{s}}}\ln\left[P_0^*\sqrt{\frac{\alpha\Sigma_2^* C_0\pi n}{4\tau F\lambda_{\mathrm{ex}}}\frac{\Delta t}{N_{\min}}(1-\sqrt{1-\mathrm{NA}^2})}\right]. \tag{11}$$

In the case of low Σ_2^* or low fluorophore concentration, the P_{f} determined from (9) may exceed the maximum permissible value P_{f}^*. This situation means that, when the noninvasivity requirements are met, the minimum necessary useful signal level cannot be reached in the specimen. The simplest solution to this problem is to increase the signal acquisition time, but this may lead to fluorophore photobleaching [17] and surface heating [10]. A quantitative analysis of z_3 values for particular dyes and approaches for increasing the imaging depth are presented in Section 3.

3. Discussion

The above section considered three factors limiting the TPFM imaging depth and presented relations for the corresponding maximum depths: z_1, z_2 and z_3. To find out which factor plays a key role in studies of a particular specimen, consider the dependence of $z_1 - z_3$ on the photon mean free path between scattering events (scattering length): $l_{\mathrm{s}} = 1/\mu_{\mathrm{s}}$. A scattering medium is commonly described by its scattering coefficient μ_{s} and the average cosine of the scattering angle g (anisotropy factor of the scattering phase function). Small-angle diffusion approximation formulas, however, contain another single-scattering characteristic: the variance of the small-angle part of the phase function, $\langle\theta^2\rangle$. To find the relation between these statistical characteristics, consider the Henyey–Greenstein scattering phase function [26, 27]

$$p_{\mathrm{HG}}(\theta) = \frac{1-g^2}{[1+g^2-2g\cos\theta]^{3/2}},$$

*Nondescanned detection means that, after the objective, the fluorescence signal enters directly the photodetector, without passing through scanning mirrors or a confocal pinhole. This allows one to avoid additional losses of the weak useful signal under nonlinear fluorescence excitation, when even scattered photons carry useful information.

normalised as follows: $\frac{1}{2}\int_0^{\pi} p_{\mathrm{HG}}(\theta)\sin\theta \mathrm{d}\theta = 1$,where θ is the scattering angle. To assess the small-angle part of the Henyey–Greenstein phase function, it can be approximated by a two-component phase function that comprises small-angle (p_1) and isotropic parts in implicit form [28]:

$$p_{\mathrm{HG}}(\theta) \simeq g p_1(\theta) + (1-g). \tag{12}$$

With this approximation, the small-angle part p_1, which contributes to the scattering within the forward hemisphere, well represents the highly directional part of the Henyey–Greenstein phase function. The variance of the small-angle part is the second moment of the function p_1, with the integration over the forward hemisphere: $\theta \in [0;\pi/2]$. For anisotropy factors above 0.7, the following asymptotic relation between $\langle\theta^2\rangle$ and g can be derived:

$$\langle\theta^2\rangle \simeq (1-g). \tag{13}$$

The other parameters needed to calculate $z_1 - z_3$ should correspond to the instrumental characteristics of standard laser scanning microscopy systems equipped with pulsed Ti:sapphire laser sources. The specimen is excited at a wavelength $\lambda_{\mathrm{ex}} = 800$ nm using a water immersion objective with a numerical aperture NA = 0.8. The excitation pulse duration is $\tau = 100$ fs, the pulse repetition frequency $F = 100$ MHz, the shape factor for a Gaussian pulse $\alpha = 0.4$ and the signal acquisition time per pixel $\Delta t = 3$ μs. The value of z_3 will be evaluated for three types of fluorophores: an endogenous substance (NADH), a common organic fluorophore (fluorescein) and semiconductor nanocrystals (quantum dots) – a new class of markers for laser scanning microscopy. The following near-IR two-photon action cross sections were reported for these fluorophores: $\Sigma^*_{\mathrm{NADH}} = 0.01$ GM [2], $\Sigma^*_{\mathrm{Fsn}} = 100$ GM [13] and $\Sigma^*_{\mathrm{QDs}} = 2\times10^4$ GM [15]. According to published data, typical intracellular concentrations of exogenous fluorophores are 10^{12} to 10^{14} mL^{-1} [29–31], and the NADH concentration reaches 10^{17} to 10^{18} mL^{-1} [32, 33].

Figure 5 plots the TPFM imaging depth limits z_1 and z_2, set by beam broadening (z_1) and near-surface fluorescence (z_2), against photon mean free path, l_s, in a scattering, nonabsorbing medium. Also presented in Fig. 5 are data for a depth equal to the transport length, $l_t = l_s/(1-g)$, which separates the small-angle and diffuse scattering regions. It can be seen that TPFM loses submicron resolution at approximately the same depth where the informative image from the focal region begins to blur because of the near-surface fluorescence. In other words, neither of the fundamental TPFM limits can be considered predominant: both the z_1 and z_2 imaging depth limits lie in the range 10–15 scattering lengths and are close to l_t. Therefore, the range of TPFM imaging depths in moderately scattering media can theoretically be extended to 1–2 millimetres.

At the same time, the instrumental limitation on the TPFM imaging depth by the low useful signal level (z_3) proves the most important. Figure 6 plots z_3 against photon mean free path for the three fluorophores above at typical TPFM conditions and realistic parameters of biological specimens. As seen, the instrumentally limited TPFM imaging depth is within $2l_s$ for the exogenous organic fluorophore (fluorescein) and $5l_s$ for the brighter colloidal quantum dots. Biological tissues range in near-IR l_s from 30 to 200 μm, which corresponds to a scattering coefficient

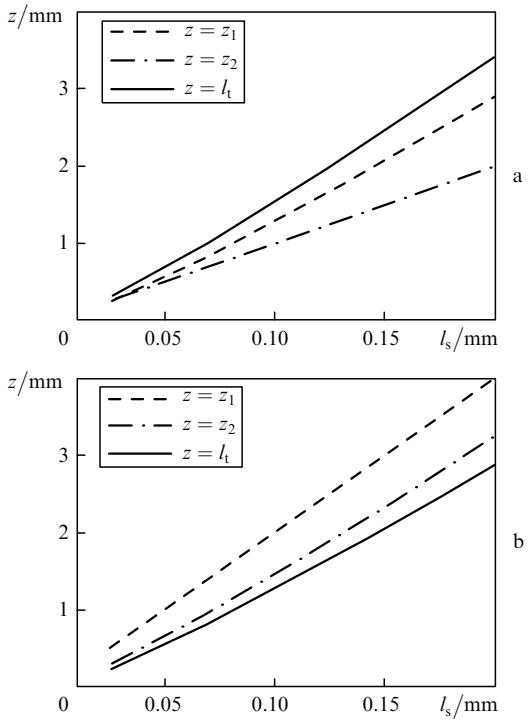

Figure 5. Maximum two-photon fluorescence microscopy imaging depths limited by beam broadening (z_1) and strong near-surface fluorescence (z_2) vs. scattering length in a medium with an anisotropy factor $g = 0.9$ (a) and 0.95 (b). Excitation wavelength $\lambda_{\mathrm{ex}} = 800$nm, average refractive index of the medium $n = 1.33$, numerical aperture of the focusing objective NA = 0.8. The solid lines show the transport length.

$\mu_s = 5 - 30$ mm^{-1}. Therefore, the instrumental limit of TPFM is 60–400 μm for organic fluorophores and 150–1000 μm for quantum dots (depending on the type of biological tissue). The excitation power P_f needed to generate the minimum useful signal is about 10 mW for the organic fluorophore and about 5 mW for quantum dots. Thus, quantum dots used as fluorescent probes reduce the

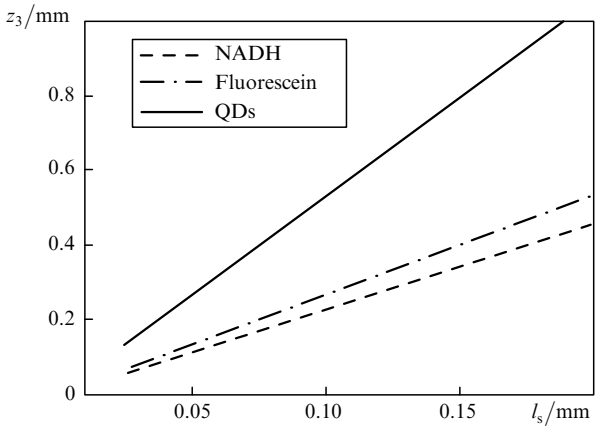

Figure 6. Maximum two-photon fluorescence microscopy imaging depth limited by the low useful signal level for three types of fluorophores: NADH (concentration, 10^{17} mL^{-1}), fluorescein (concentration, 2×10^{13} mL^{-1}) and colloidal quantum dots (QDs; concentration, 2×10^{13} mL^{-1}). Excitation wavelength $\lambda_{\mathrm{ex}} = 800$nm, average refractive index of the medium $n = 1.33$, numerical aperture of the focusing objective NA = 0.8.

probability of specimen photodamage in the focal region. At the same time, the average power in specimens labelled with quantum dots should be maintained below 5 mW. Otherwise, the two-photon absorption in the quantum dots may saturate, cancelling out the gain in imaging depth and adversely affecting the spatial resolution [2, 34]. The two-photon fluorescence signal of endogenous fluorophores with a two-photon absorption cross section of the order of 0.01 GM is difficult to detect at concentrations below 10^{16} mL^{-1} because, even at an excitation power of 10 mW, no photons may reach the detector during the signal acquisition time. At much higher concentrations (e.g. in mitohondrial accumulations), the two-photon fluorescence signal of an endogenous fluorophore may approach the fluorescence signal of moderately bright organic dyes (Fig. 6). This enables imaging of unstained biological tissues using their two-photon autofluorescence at depths exceeding the photon mean free path. On the other hand, autofluorescence from regions with an increased endogenous fluorophore concentration may hinder the observation of two-photon fluorescence of exogenous dyes that label particular elements of cells or biological tissues. To avoid this, one should either detune the fluorophore – fluorophore excitation wavelength from two-photon autofluorescence or select dyes that differ markedly in fluorescence spectrum from endogenous fluorophores.

Note that the z_3 values calculated by Eqn (11) and presented in Fig. 6 should be viewed as approximate because they were obtained for some average fluorophore concentrations. In each particular case, the local concentration may be substantially higher or lower, depending on fluorophore accumulation features. According to (11), however, changes in concentration by several times will cause changes in z_3 by only a few or tens of percent. The z_3 limit can be considerably raised by increasing the inverse of the pulse duty factor, $S = (\tau F)^{-1}$, and hence the excitation peak power, while maintaining the average power unchanged. This can be achieved by reducing the repetition rate of femtosecond pulses using a regenerative amplifier as the excitation source. State-of-the-art regenerative amplifiers enable a reduction in pulse repetition rate by three orders of magnitude [35]. The peak power rises, however, in proportion to the inverse of the pulse duty factor, with a substantial increase in the probability of optical breakdown of the biological specimen in the focal region because, at an average focal power in the milliwatt range, the local intensity exceeds 10 TW cm^{-2}. With no consideration for the possibility of nonlinear photodamage to biological tissues, the use of a regenerative amplifier enables the instrumentally limited TPFM imaging depth in specimens labelled with colloidal quantum dots to be increased to $8l_s$, which approaches the fundamental TPFM limits set by z_1 and z_2.

4. Conclusions

This work has examined three main factors that limit the imaging depth in two-photon fluorescence microscopy of strongly scattering biological tissues. Two fundamental limitations are identified, one related to the influence of multiple small-angle scattering on the shape of the highly focused excitation beam, and the other to the near-surface fluorescence in the scattering specimen. These factors limit the TPFM imaging depth to 10 – 15 scattering lengths, which is close to the transport length. The most stringent limitation is, however, placed by the low fluorescence signal level at large depths because of the exponential attenuation of the excitation power, the low two-photon excitation efficiency and the insufficient fluorophore concentration. One way to increase the imaging depth up to the fundamental limit is to use fluorophores with the largest two-photon absorption cross section (colloidal quantum dots) and a regenerative amplifier in order to raise the excitation peak power, but the latter involves a high risk of optical breakdown of biological specimens.

Acknowledgements. This work was supported in part by the Federal Agency for Science and Innovation (State Contract No. 02.740.11.086), the Russian Foundation for Basic Research (Grant Nos 08-02-01293, 09-02-97083 and 09-04-12254) and the RF President's Grants Council (Support to Young Candidates of Science Programme, Grant No. MK-698.2009.2).

References

1. Denk W., Strickler J.H., Webb W.W. *Science*, **248**, 73 (1990).
2. Xu C., Webb W.W., in *Topics in Fluorescence Spectroscopy* (New York: Plenum Press, 1997) Vol. 5.
3. So P.T.C., Dong C.Y., Masters B.R., Berland K.M. *Annu. Rev. Biomed. Eng.*, **2**, 399 (2000).
4. Zipfel W.R., Williams R.M., Webb W.W. *Nat. Biotechnol.*, **21**, 1368 (2003).
5. Helmchen F., Denk W. *Nat. Methods*, **2**, 932 (2005).
6. *Ultrashort Laser Pulses in Biology and Medicine*. Ed. by M. Braun, P. Gilch, W. Zint (Berlin: Springer, 2008).
7. Koenig K., Ehlers A., Riemann I., Schenkl S., Bueckle R., Kaatz M. *Microsc. Res. Tech.,* **70**, 398 (2007).
8. Gelikonov G.V., Dolin L.S., Sergeeva E.A., Turchin I.V. *Izv. Vyssh. Uchebn. Zaved., Ser. Radiofiz.*, **46**, 628 (2003) [*Radiophysics and Quantum Electronics*, **46**, 565 (2003)].
9. Kirillin M.Yu., Priezzhev A.V., Myllylä R. *Kvantovaya Elektron.*, **38**, 570 (2008) [*Quantum Electron.*, **38**, 570 (2008)].
10. Tuchin V.V. *Tissue Optics: Light Scattering Methods and Instruments for Medical Diagnosis* (Bellingham: SPIE Optical Engineering Press, 2000).
11. Ishimaru A. *Wave Propagation and Scattering in Random Media* (New York: Academic, 1978; Moscow: Mir, 1981) Vol. 1.
12. Theer P., Denk W. *J. Opt. Soc. Am. A*, **23**, 3139 (2006).
13. Xu C., Webb W.W. *J. Opt. Soc. Am. B*, **13**, 481 (1996).
14. Zipfel W.R., Williams R.M., Christie R., Nikitin A.Y., Hyman B.T., Webb W.W. *Proc. Nat. Acad. Sci. USA,* **100**, 7075 (2003).
15. Larson D.R., Zipfel W.R., Williams R.M., Clark S.W., Bruchez M.P., Wise F.W., Webb W.W. *Science*, **300**, 1434 (2003).
16. Oheim M., Beaurepaire E., Chaigneau E., Mertz J., Charpak S. *J. Neurosci. Methods,* **111**, 29 (2001).
17. Pawley J.B. (Ed.) *Handbook of Biological Confocal Microscopy* (Berlin: Springer, 2006).
18. Zege E.P., Ivanov A.V., Katsev I.L. *Image Transfer Through a Scattering Medium* (Berlin: Springer-Verlag, 1991; Minsk: Nauka i Tekhnika, 1985).
19. Kokhanovsky A.A. *Meas. Sci. Technol.*, **13**, 233 (2002).
20. Dolin L.S. *Izv. Vyssh. Uchebn. Zaved., Ser. Radiofiz.*, **41**, 1258 (1998) [*Radiophysics and Quantum Electronics*, **41**, 850 (1998)].
21. Leray A., Odin C., Le Grand Y. *Opt. Commun.*, **281**, 6139 (2008).
22. Sheppard C.J.R., Gan X., Gu M., Ray M., in *Handbook of Biological Confocal Microscopy* (New York: Plenum Press, 1995).
23. Dixon A., Heinlein T., Wolleschensky R. *Springer Ser. Fluoresc.,* **6**, 3 (2008).
24. Koenig K., Becker T.W., Fischer P., Riemann I., Halbhuber K.-J. *Opt. Lett.*, **24**, 113 (1999).

25. Hopt A., Neher E. *Biophys. J.*, **80**, 2029 (2001).
26. Henyey L.G., Greenstein J. L. *Astrophys. J.*, **93**, 70 (1941).
27. Jacques S.L., Alter C.A., Prahl S.A. *Lasers Life Sci.,* **1**, 309 (1987).
28. Dolin L.S., Sergeeva E.A. *Izv. Vyssh. Uchebn. Zaved., Ser. Radiofiz*., 44, 931 (2001) [*Radiophysics and Quantum Electronics*, **44**, 858 (2001)].
29. Vukojevic V., Heidkamp M., Ming Y., Johansson B., Terenius L., Rigler R. *Proc. Nat. Acad. Sci. USA*, **105**, 18176 (2008).
30. Chang E., Thekkek N., Yu W.W., Colvin V.L., Drezek R. *Small*, **2**, 1412 (2006).
31. www.probes.invitrogen.com/media/pis/mp19011.pdf.
32. Yu Q., Heikal A.A. *J. Photochem. Photobiol., B,* **95**, 46 (2009).
33. Lin S.J., Ford E., Haigis M., Liszt G., Guarente L. *Genes Dev.,* **18**, 12 (2004).
34. Katichev A.R., Sergeeva E.A. *Opt. Spektrosk*., **107**, 887 (2009) [*Opt. Spectrosc*., **107**, 839 (2009)].
35. Theer P., Hasan M.T., Denk W. *Opt. Lett*., **28**, 1022 (2003).